Eur. Phys. J. Plus (2022) 137:1377
https://doi.org/10.1140/epjp/s13360-022-03610-w

THE EUROPEAN PHYSICAL JOURNAL PLUS

Regular Article

Critical behaviors of transverse Ising ferromagnet with random bond and random longitudinal magnetic field

J. Kple[1,2], **E. Albayrak**[3,a], **T. D. Oke**[1], **F. Hontinfinde**[1,2]

[1] Institute of Mathematic and Physical Sciences (IMSP), Dangbo, Republic of Benin
[2] Department of Physics, University of Abomey-Calavi, Godomey, Republic of Benin
[3] Department of Physics, Erciyes University, 38039 Kayseri, Turkey

Received: 2 November 2022 / Accepted: 19 December 2022

Abstract The transverse Ising model with bimodal random bond dilution and trimodal random longitudinal magnetic field was studied in terms of the effective-field theory (EFT) with correlations for a finite-cluster. The nearest-neighbor spins are assumed to be interacting randomly either ferromagnetically with probability p or the interaction between them are turned off with probability $(1-p)$. It is also assumed that half of the spins are under the influence of longitudinal magnetic field with equal probability t/2 along z-axis having the values of $+H$ and $-H$ while the other half of spins is free of H with probability $1-t$. The effects of changing the probabilities p and t, and the magnitudes of transverse and longitudinal magnetic fields for the magnetization components under temperature variations were examined in detail to obtain the possible phase diagrams of the model. It was obtained that the model exhibits both second- and first-order phase transitions, in addition to the tricritical points and reentrant behaviors for the first- and second-order phase transition temperature lines.

1 Introduction

After the introduction of Ising model for the spin-1/2 systems in one-dimensional case [1], it has evolved in many ways. The spin and space dimensions were increased, some new parameters added, and some parameters are randomized in various directions and so on.

The spin-1/2 transverse Ising model (TIM), i.e., the Ising model with transverse field (TF), was considered in some works as follows: The effect of the surface TF on the order–disorder layering transitions was investigated using the mean field theory (MFT) and the finite cluster approximation (FCA) [2]. The temperature and TF dependence of entropy and specific heat of ferroics were investigated using the TIM within the MFT and Gaussian spin fluctuation approximations [3]. The Heisenberg ferromagnet with TF was studied by combining the two-spin cluster expansion with the perturbation theory [4]. The alternating magnetic superlattice was examined using the EFT with probability distribution [5]. The magnetization properties of an antiferromagnet consisting of two alternating layers in a TIM were studied by the use of the EFT with correlations and MFT [6, 7]. In addition, the two-sublattice model on an anisotropic square lattice was considered in both longitudinal and transverse fields by using the EFT [8]. The two-dimensional anisotropic antiferromagnetic (AFM) model in both uniform longitudinal field and uniform TF was studied by employing a mean-field (MF) variational approach based on Bogoliubov inequality for the free energy [9] and in the EFT with correlation [10]. The AFM model with the same external constraints was considered in the EFT with finite cluster in two- [11] and three-dimensional cases [12]. The Ising film in a TF within the framework of EFT was examined as a function of exchange interactions, TF and film thickness [13]. The two-sublattice metamagnet at finite temperatures in a mixed longitudinal field and TF was investigated by the use of the EFT with correlations [14]. The TIM with four-spin interactions was studied within the FCA on honeycomb and square lattices [15]. The frustrated $J_1-J_2-J_3$ TIM antiferromagnet on a honeycomb lattice was also examined by using in the EFT [16]. The frustrated Ising antiferromagnet with first- and second-nearest-neighbor interactions was studied on square lattices in a TF by using an EFT with correlations based on a single-spin approximation [17].

The Ising model with site or bond dilutions (BD) was also examined in many works given as follows. The random interactions were investigated within the framework of the EFT using an improved configurational averaging procedure [18]. The amorphization was studied within the EFT for a cubic lattice with $N=6$ [19]. The site-bond-correlated dilution was proposed to account for the differences experimentally observed by nuclear-magnetic-resonance measurements between random-diluted $KNi_pMg_{1-p}F_3$ and the isostructural system $KMn_pMg_{1-p}F_3$ [34]. Using Monte Carlo (MC) simulation techniques, the 2D site-diluted Ising model was also studied [22]. The non-metallic compounds $ZnCr_{2p}Al_{2-2p}S_4$ and $Zn_{1-p}Cd_pCr_2Se_4$ were considered on the spinel B site lattice

[a] e-mail: albayrak@erciyes.edu.tr (corresponding author)

Published online: 27 December 2022

with competitive exchange interactions [23]. The $LiHo_xY_{1-x}F_4$ magnetic material in a TF perpendicular to the Ising spin direction was used to study tunable quantum phase transitions in a random disordered system [24]. A BD model with temperature-dependent concentration of bonds was introduced to simulate the excitations of bond degrees of freedom as in covalently bonded network liquids arising from the thermal electronic transitions between bonding and antibonding electronic states [25]. The effect of long-range connections on the infinite-randomness fixed point associated with the quantum phase transitions in a TIM was considered [26]. A two-stage approach of the Wang–Landau algorithm was applied to investigate the critical properties of the 3D Ising model with quenched bond randomness [27]. It was found that the random-bond model on the square lattice has several disordered critical points depending on the probability distribution of the bonds [28]. The FM model on a square lattice in the presence of randomness in the form of BD was studied by Wang–Landau algorithm of MC method [29]. The BD effects on the critical temperatures, phase diagrams and the magnetization behaviors of the isotropic and anisotropic quantum Heisenberg model were investigated [30]. The order-parameters were investigated to study the phase diagrams of the $\pm J$ model in the lowest approximation of the cluster variation method (LACVM) [31].

As an other parameter, the randomization of longitudinal magnetic field was also considered. The phase diagram of the random field Ising model (RFIM) on the Bethe lattice with a symmetric dichotomous RF was investigated with respect to the transition between ferromagnetic (FM) and paramagnetic (PM) regimes [32]. The diamond family of hierarchical lattices with arbitrary dimension and scaling factor of 2 was considered for the Gaussian and discrete delta-bimodal initial symmetric probability distributions [33]. The RFIM model was examined on a honeycomb lattice by means of the EFT, and the phase diagrams were obtained in the $T - H$ plane for clusters with one spin in a finite-size cluster scheme [34, 35]. The phase diagrams and thermodynamic parameters for the Gaussian RFIM on spherical lattice were studied by the MFT [36]. The RFIM under bimodal and Gaussian distributions was investigated using a finite connectivity technique [37]. The Heisenberg model with fluctuating bond interactions between nearest neighbors and in the presence of a RF with the asymmetric and anisotropic trimodal probability distribution was investigated by the EFT based on two-spin cluster [38]. The RFIM in an external magnetic field with a computationally efficient graph-cut method was used to study ground state (GS) morphologies with Gaussian, uniform and bimodal distributions [39]. The Ising model in the presence of a RF was investigated within the MFT based on Landau expansion with the trimodal probability distribution [40]. The RFIM in bimodal form with four-spin interactions was studied within the FCA on square and simple cubic lattices [41]. As a result of the interplay between the intrinsic off-diagonal terms of the dipolar interaction and an applied transverse field, it was shown that the diluted $LiHo_xY_{1-x}F_4$ system at $x > 0.5$ is equivalent to a ferromagnet in a longitudinal RF [42]. The Blume–Capel (BC) model was studied under the effect of a bimodal [43] and trimodal [44] RF with equal probabilities on the Bethe lattice in terms of the exact recursion relations. The bimodal RF with equal probability was investigated by using the lowest approximation of the cluster-variation method in the BC model [45].

In addition to these, some works also investigated the effects of randomization in two parameters simultaneously. The 2D random site dilution and random-bond Ising model was studied for the critical behaviors at the PM-FM transition using the renormalization group method [46]. The critical behavior of bond- and site-diluted TIM on a square lattice with spin-1/2 was investigated by the FCA [47]. The random crystal and magnetic field effects on hysteresis loops and phase transitions of the BC model were analyzed by means of the CVM [48].

Since all these works cited above have brought out some characteristics of these models, we have decided to study the TIM with bimodal random bond dilution and trimodal random longitudinal magnetic field in terms of the EFT with correlations for a finite-cluster. The spins interact ferromagnetically with probability p or it is turned off with probability $(1 - p)$ randomly for the neighboring spins, and the half of the spins are under the influence of longitudinal magnetic field with equal probability $t/2$ along the z-axis as $+H$ and $-H$ while the other half of spins is free of H with probability $1 - t$. The effects of changing the probabilities p and t, and the magnitudes of transverse and longitudinal magnetic fields for the magnetization components under temperature variations were examined in detail to obtain the possible phase diagrams of the model.

The remaining part of the work is constructed as follows: the model and its solution within the EFT is introduced in Sect. 1, thermal variations of magnetization components are explored in Sect. 2, the phase diagrams and their detailed analysis are presented in Sect. 3, and the last section contains our findings and a brief summary.

2 The model and its EFT solution

The transverse spin-1/2 Ising model with bond dilution and a random longitudinal magnetic field is considered for the Hamiltonian of the system given in the form as

$$\mathcal{H} = \sum_{\langle i,j \rangle} J_{ij} S_i^z S_j^z - \Omega \sum_i S_i^x - \sum_i h_i S_i^z, \tag{1}$$

where S_i^x and S_i^z are the x- and z-components of the spin-1/2 operators at site i, respectively. J_{ij} is the nearest-neighbor bilinear exchange interaction parameter chosen to be FM, i.e., $(J_{ij} < 0.0)$, which is either turned on with probability p or off with $1 - p$ throughout the lattice. It has the following independent bond-dilution probability distribution:

$$P(J_{ij}) = p\delta(J_{ij} + J) + (1 - p)\delta(J_{ij}), \tag{2}$$

where p stands for the bond concentration or probability with $0 \leq p \leq 1$. Each spin is also assumed to be subjected to a random longitudinal magnetic field H_i governed by the following trimodal symmetric distribution law:

$$P(h_i) = \frac{1}{2}t[\delta(h_i - H) + \delta(h_i + H)] + (1 - t)\delta(h_i), \tag{3}$$

where two portions, $t/2$ of the spins are under the influence of the longitudinal magnetic field along $+H$ and $-H$ directions while the other portion $(1 - t)$ of spins is free of the influence of this field, i.e., $H = 0$, with $0 \leq t \leq 1$. Within the EFT with correlations for a finite-cluster, in particular, for a cluster with $N = 1$ spin, we rewrite the Hamiltonian by considering a selected single spin labeled 0 and its neighboring spins with which it directly interacts in the following form:

$$-\beta\mathcal{H}_0 = \sum_{j=1}^{q} \beta(h_0 - J_{0j}S_j^z)S_0^z + \beta\Omega S_0^x, \tag{4}$$

where q refers to the lattice coordination number. In order to evaluate the thermal average of spin operators $\langle S_0^z\rangle$ and $\langle S_0^x\rangle$, this single-site cluster Hamiltonian can readily be diagonalized and according to the generic identity due to Callen-Suzuki [49, 50] one finds:

$$m_0^z = \left\langle \frac{h_0 - x_0}{\sqrt{(h_0 - x_0)^2 + \Omega^2}} \tanh\left(\beta\sqrt{(h_0 - x_0)^2 + \Omega^2}\right)\right\rangle, \tag{5}$$

$$m_0^x = \left\langle \frac{\Omega}{\sqrt{(h_0 - x_0)^2 + \Omega^2}} \tanh\left(\beta\sqrt{(h_0 - x_0)^2 + \Omega^2}\right)\right\rangle \tag{6}$$

where $x_0 = \sum_{j=1}^{q} J_{0j}S_j^z$, and $\langle\cdots\rangle$ indicates the usual canonical thermal average.

By introducing the differential operator technique [51], $\exp(\alpha D_x)F(x) = F(x + \alpha)$ where $D_x = \frac{\partial}{\partial x}$ is the differential operator, together with the Van der Waerden identity [52] for the two-state spin system, namely, $\exp(\alpha S_i^z) = \cosh(\alpha) + S_i^z \sinh(\alpha)$, Eqs.(5)–(6) lead to the following expectation expressions:

$$m_0^z = \left\langle \prod_{j=1}^{q} \Big(\cosh(J_{ij}D_x) + S_j^z \sinh(J_{ij}D_x)\Big)\right\rangle F(x)|_{x=0}, \tag{7}$$

and

$$m_0^x = \left\langle \prod_{j=1}^{q} \Big(\cosh(J_{ij}D_x) + S_j^z \sinh(J_{ij}D_x)\Big)\right\rangle G(x)|_{x=0} \tag{8}$$

with

$$F(x) = \frac{h_i - x}{\sqrt{(h_i - x)^2 + \Omega^2}} \tanh\left(\beta\sqrt{(h_i - x)^2 + \Omega^2}\right) \tag{9}$$

and

$$G(x) = \frac{\Omega}{\sqrt{(h_i - x)^2 + \Omega^2}} \tanh\left(\beta\sqrt{(h_i - x)^2 + \Omega^2}\right). \tag{10}$$

The decoupling approximation of the type $\langle S_i^z S_j^z \cdots S_l^z\rangle \equiv \langle S_i^z\rangle\langle S_j^z\rangle \cdots \langle S_l^z\rangle$ for $i \neq j \cdots \neq l$, which corresponds to the Zernike approximation [53], has also been introduced for the multispin correlation functions which appear by expanding the right-hand sides of Eqs.(7)–(8). Hence, the longitudinal and transverse magnetizations can be evaluated from the following equations:

$$m_z = \sum_{l=0}^{q} A_l(T, J_{ij}, h_i, \Omega)(m_z)^l, \tag{11}$$

and

$$m_x = \sum_{l=0}^{q} B_l(T, J_{ij}, h_i, \Omega)(m_z)^l, \tag{12}$$

with

$$A_l(T, J_{ij}, h_i, \Omega) = \frac{q!}{l!\,(q - l)!}\alpha_x^{q-l}\beta_x^l F(x)|_{x=0}, \tag{13}$$

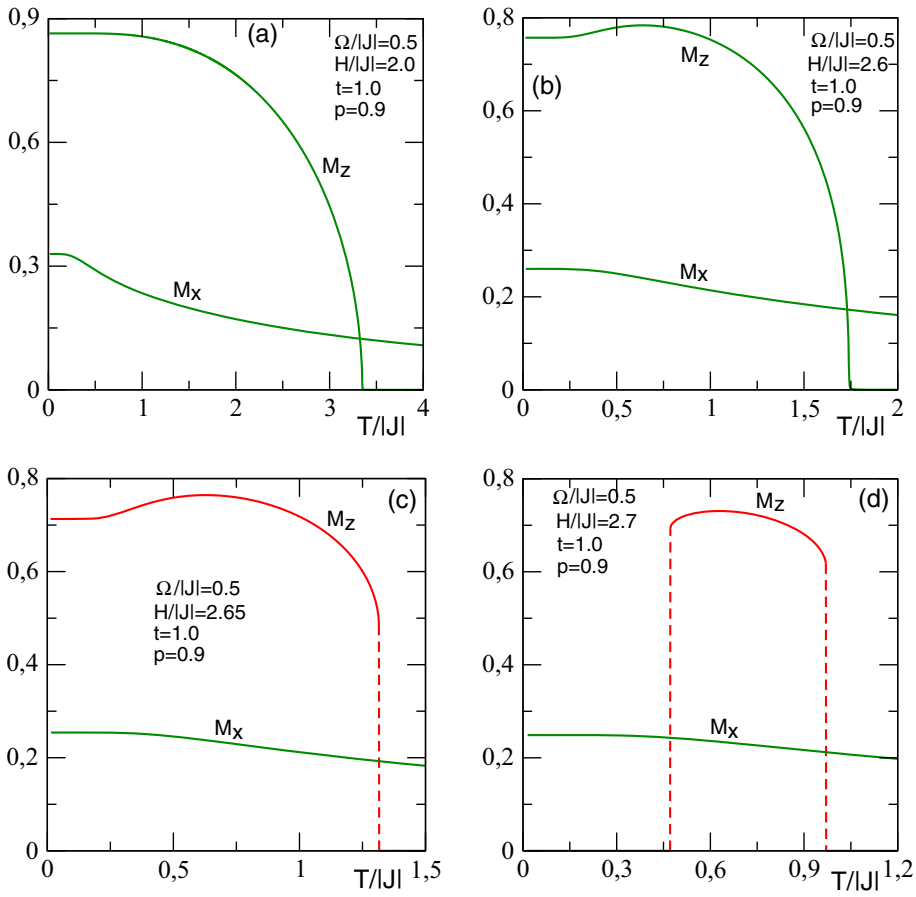

Fig. 1 Thermal variations of the longitudinal and transverse magnetizations M_z and M_x on a simple cubic lattice for $p = 0.9$, $t = 1.0$ and $\Omega/|J| = 0.5$ when **a** $H/|J| = 2.0$, **b** $H/J = 2.6$, **c** $H/|J| = 2.65$ and **d** $H/|J| = 2.7$

and

$$B_l(T, J_{ij}, h_i, \Omega) = \frac{q!}{l!\,(q-l)!}\alpha_x^{q-l}\beta_x^l G(x)|_{x=0}, \tag{14}$$

where $\alpha_x = \cosh(J_{ij}D_x)$ and $\beta_x = \sinh(J_{ij}D_x)$.

According to the distribution laws (2) and (3), one must perform the bond dilution average of J_{ij} and the random average of h_i. Thus, by the use of Eqs.(11 – 12), the longitudinal and transverse site magnetizations are given in the following forms:

$$M_z = \int\int m_z\, P(J_{ij})P(h_i)dJ_{ij}dh_i, \tag{15}$$

$$M_x = \int\int m_x\, P(J_{ij})P(h_i)dJ_{ij}dh_i, \tag{16}$$

which include the effects of bond-dilution and the random longitudinal magnetic field and thus, these coupled equations can be solved numerically.

We have studied the thermal variations of the longitudinal and transverse magnetizations to deduce the phase diagrams of the model in the case of a simple cubic lattice ($q = 6$) which corresponds to the three-dimensional structure. This dimension is considered, not only to explore the physical properties for a higher coordination number, but also it appears in the case of experimental research as one of the most relevant dimension.

In order to obtain the ground state (GS) phase diagrams, we follow the same procedure as described for $T \neq 0.0$ above. The magnetizations m_z and m_x defined in Eqs. (11 – 12) are evaluated with

$$A_l(J_{ij}, h_i, \Omega) = \frac{q!}{l!\,(q-l)!}\alpha_x^{q-l}\beta_x^l F_0(x)|_{x=0} \tag{17}$$

and

$$B_l(J_{ij}, h_i, \Omega) = \frac{q!}{l!\,(q-l)!}\alpha_x^{q-l}\beta_x^l G_0(x)|_{x=0} \tag{18}$$

where $\alpha_x = \cosh(J_{ij}D_x)$, $\beta_x = \sinh(J_{ij}D_x)$ and $F_0(x)$ and $G_0(x)$ are the functions in Eqs. (9) and (10) at $T = 0$.

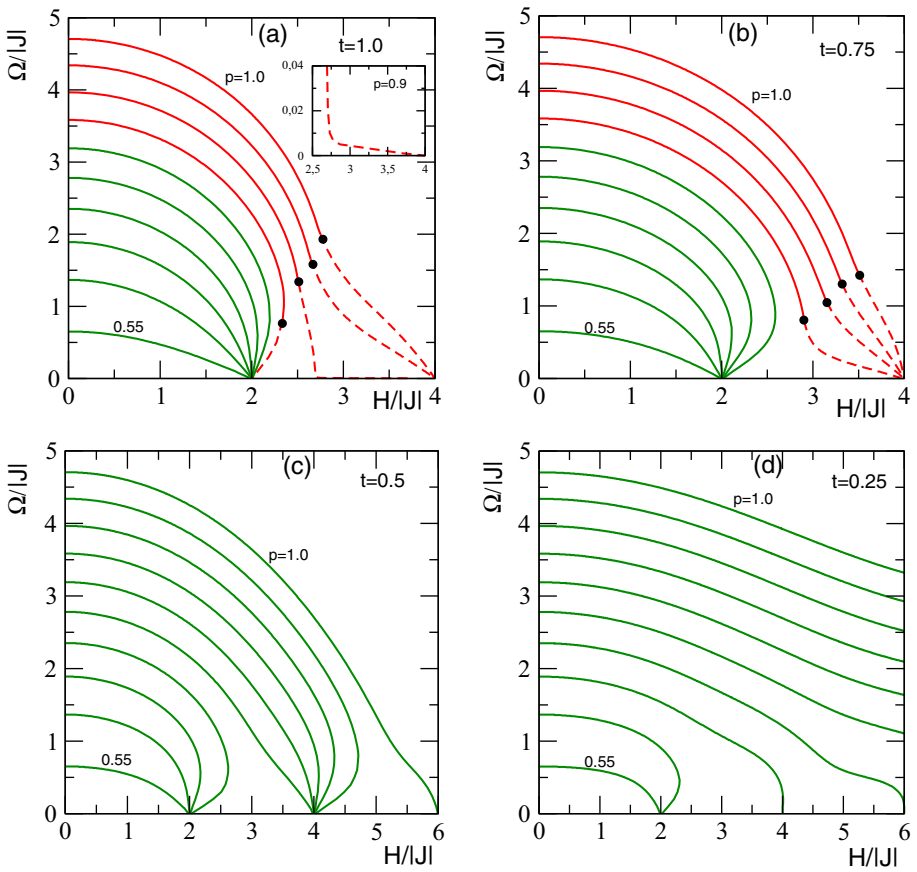

Fig. 2 Ground state phase diagrams of the transverse Ising ferromagnet in a bond-diluted and a random longitudinal magnetic field on the $(H/|J|, \Omega/|J|)$ plane with **a** $t = 1.0$, **b** $t = 0.75$, **c** $t = 0.5$ and **d** $t = 0.25$. Each curve is associated with one value of the bond dilution concentration p which decreases from 1.0 with the increment of 0.05. Solid (dashed) lines are the second- (first) order transition lines. Red ones are associated with phase boundaries with TCPs (circles)

3 Thermal variations of the magnetization components

In order to obtain the phase diagrams, a detailed thermal analysis of magnetization components is necessary. Since the TF is along the $x-$axis, the corresponding magnetization component, M_x, never goes to zero as long as $\Omega/|J| \neq 0.0$. Even if the longitudinal RF is not zero, in the trimodal distribution half of the spins are under $H/|J| = 0.0$ and the rest have the same probability of being up or down, therefore, M_z does not vanish giving rise to possible phase transitions [43, 44]. When $p = 1$, the BD is turned off and all the sites interact ferromagnetically. In the contrary, when $p = 0$, all the bonds are broken with no interactions between the spins.

Figure 1(a) shows that M_z presents second-order phase transitions between the FM phase and the PM one. M_x continuously gets smaller as the temperature increases. Similar behaviors are identified in Fig. 3 and 4 of [19] and Fig. 1 of [3]. In Fig. 1(b), the same behaviors are observed, but now M_z first increases at low $T/|J|$ with respect to its $T/|J| = 0.0$ value and then, decreases with increasing temperature. As can be seen from Figs. 1(c) and (d), this behavior becomes more pronounced as $H/|J|$ increases. In panel (c), M_z shows a first-order phase transition at temperature T_t between the FM phase and the PM one. Fig. 1(d) shows the PM phase at low $T/|J|$ then M_z appears at the first T_t, as $T/|J|$ increases, it again disappears at the second T_t, entering into the PM phase again. Thus, one sees PM-FM-PM phases in sequence. A similar behavior is also observed in Fig. 3 of [19] but with continuous transitions. Therefore, a reentrant behavior may be observed for the T_c- and T_t-lines in the phase diagrams.

4 The phase diagrams in various planes

The ground state (GS) phase diagrams are illustrated on the $(H/|J|, \Omega/|J|)$ planes for different values of the parameter t and varying the values of p as shown in Fig. 2. The figure shows a shrinking of the FM phase regions as p decreases. Thus, a critical value p_c exists for the disappearance of field-induced magnetic ordering. Our calculations give $p_c \simeq 0.534$ for all values of $t > 0.0$. Variations of p are followed by pronounced qualitative changes in the phase diagrams. Tricritical points (TCP) are obtained for higher values of t. TCP is absent for $t < 0.658$. Hence, for $t = 0.5$ and 0.25, (Figs. 2(c) and (d)), the system does not exhibit first-order phase transitions as well as TCPs for any values of the system parameters p, $\Omega/|J|$ and $H/|J|$. It is also observed that the longitudinal field (LF) takes two fixed values at zero TF for $t = 1.0$ and 0.75 when p varies while three fixed values are obtained for $t = 0.5$ and 0.25. Indeed, for $t = 1.0$, one observes one fixed point at low $H/|J|$ with the mixture of continuous (Ω_c) and discontinuous (Ω_t) phase

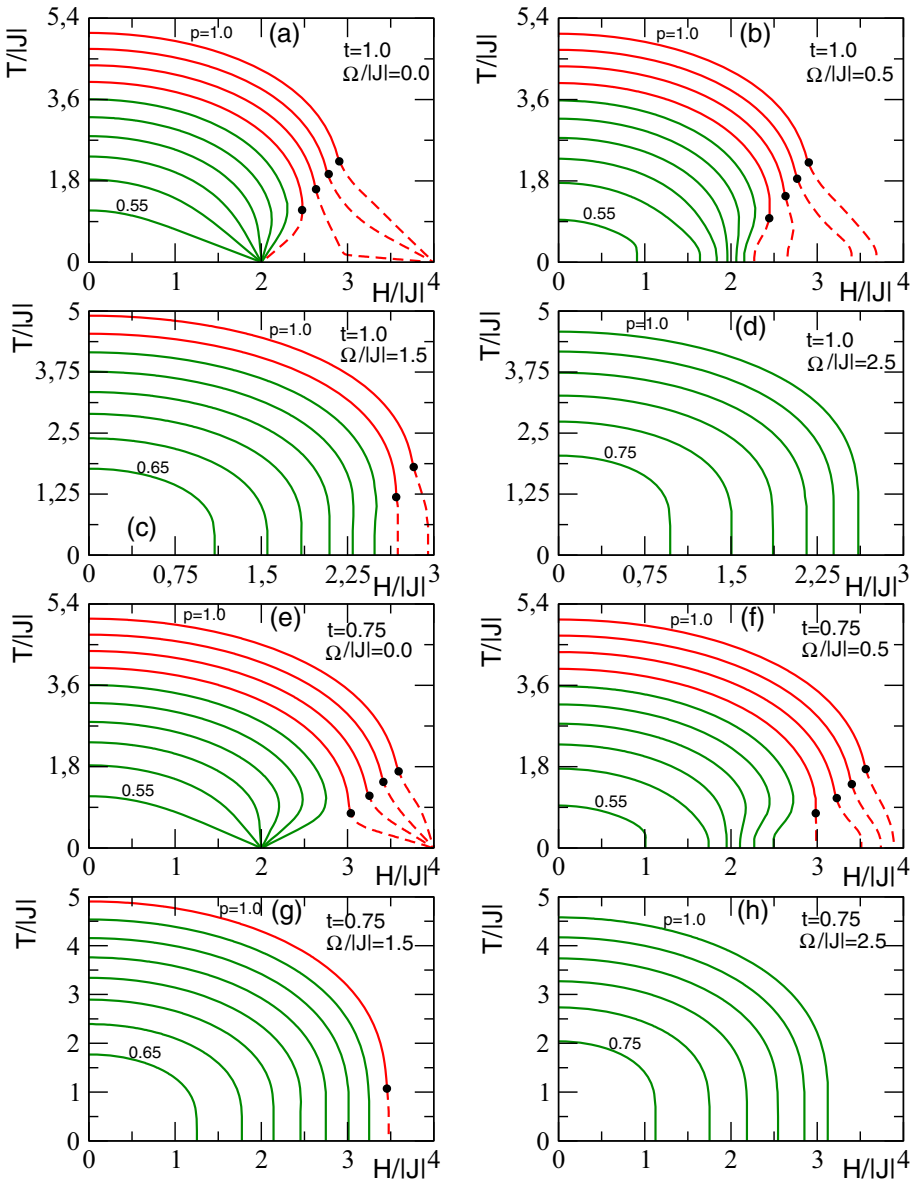

Fig. 3 Phase diagrams of the transverse Ising ferromagnet in a bond-diluted and a random longitudinal magnetic field on the $(H/|J|, \Omega/|J|)$ plane for (*i*) $t = 1.0$ when **a** $\Omega/|J| = 0.0$, **b** $\Omega/|J| = 0.5$, **c** $\Omega/|J| = 1.5$ and **d** $\Omega/|J| = 2.5$ and (*ii*) $t = 0.75$ with **e** $\Omega/|J| = 0.0$, **f** $\Omega/|J| = 0.5$, **g** $\Omega/|J| = 1.5$ and **h** $\Omega/|J| = 2.5$. Each curve is associated with one value of the bond dilution concentration p which decreases from 1.0 with the increment of 0.05. Solid (dashed) lines are the second- (first) order transition lines. Red ones are associated with phase boundaries with TCPs (circles)

transitions lines and another one at higher values of $H/|J|$ with only Ω_t-lines. When $t = 0.75$, the variations of p show two fixed values with only Ω_c-lines at low $H/|J|$ and with only Ω_t-lines at higher $H/|J|$. The three fixed values of LF obtained for $t = 0.5$ and 0.25 are associated with Ω_c-lines: In Fig. 2(c), the TF decreases gradually from its higher values for higher p as $H/|J|$ increases and vanishes at three critical values of $H/|J|$, namely 2.0, 4.0 and 6.0 for $0.55 \leq p \leq 0.70$, $0.75 \leq p \leq 0.95$ and $p = 1.0$, respectively. A similar behavior is obtained in Fig. 2(d) when $t = 0.25$, except that, $\Omega/|J|$ decreases but does not vanish for any value of $p > 0.7$, i.e., the second-order phase transition lines extend to $H/|J| \rightarrow +\infty$. It is then obvious that with the decrease in the parameter t, the effect of $H/|J|$ on the system becomes more important. The range of magnetic ordering phase in the system is enlarged.

Now, we present the thermal phase diagrams of the model. In Figs. 3 and 4, some features of the phase transitions lines are exhibited. As seen in Fig. 3(a), as $H/|J|$ increases, the phase boundary associated with the pure case ($p = 1.0$) exhibits a TCP at which a continuous (T_c) line meets a discontinuous (T_t) phase transition line which in turn depresses to zero at $H/|J| = 4.0$. Similar trends are also observed for some other values of p. For $p = 0.85$, the TCP is also obtained and the phase boundary declines and exhibits a bulge. Further, the T_t-lines now disappear at $H/|J| = 2.0$. As p decreases, the TCPs shift to lower values of $H/|J|$ and $T/|J|$. For $0.55 < p < 0.816$, the topology of the phase diagram changes and the system shows T_c-lines with associated temperatures reduced to zero at $H/|J| = 2.0$. The second-order reentrant behavior is also observed for $0.729 < p < 0.816$ while for $0.55 \leq p \leq 0.729$, this phenomenon disappears. In Fig. 3(b), it is barely visible that the phase diagram exhibits a first-order zigzag reentrant profile for $p = 0.9$ and a second-order reentrance for $p = 0.8$. The phase transition and TCP temperatures decrease with increasing values of TF as seen in Fig. 3(c) and the TCP as well as the reentrant behavior are completely suppressed for large values

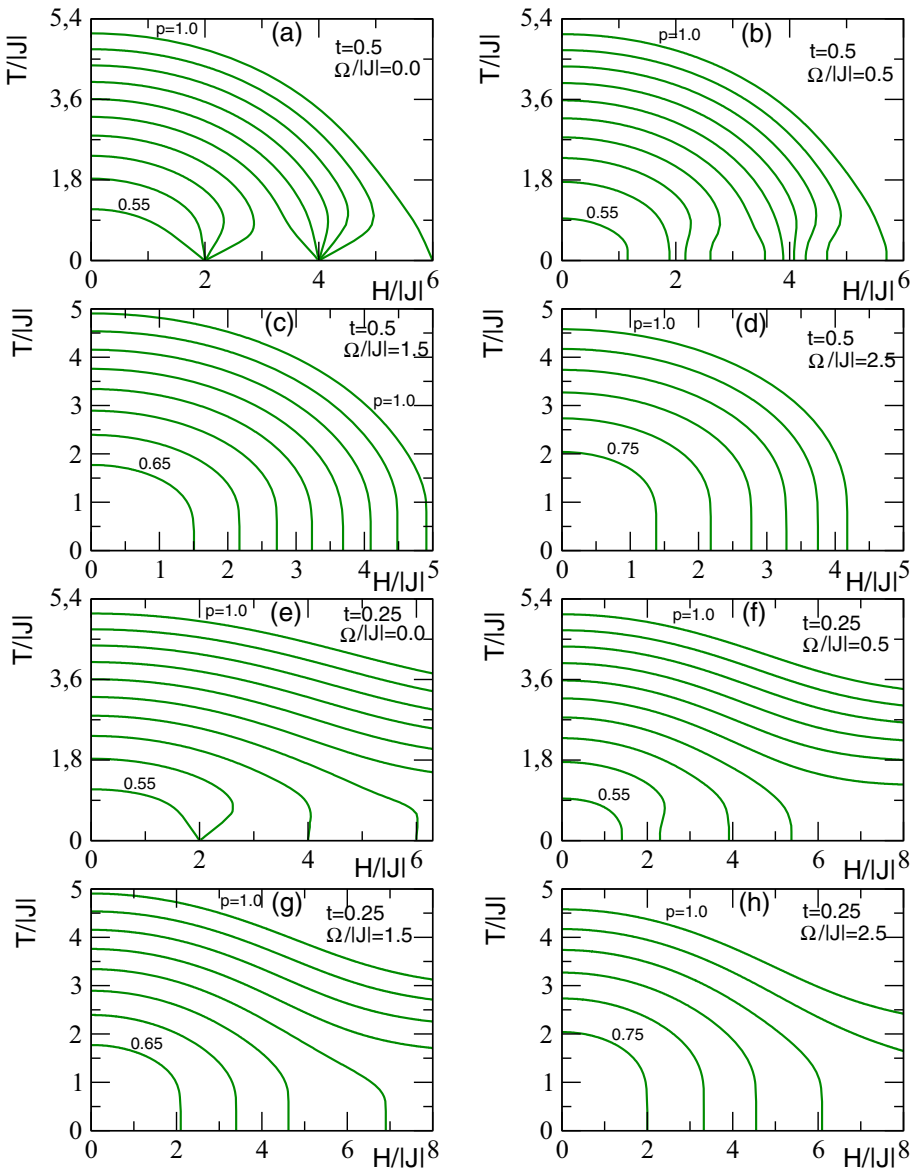

Fig. 4 Phase diagrams of the transverse Ising ferromagnet in a bond-diluted and a random longitudinal magnetic field on the ($H/|J|$, $T/|J|$) plane for (i) $t = 0.5$ with **a** $\Omega/|J| = 0.0$, **b** $\Omega/|J| = 0.5$, **c** $\Omega/|J| = 1.5$ and **d** $\Omega/|J| = 2.5$ and (ii) $t = 0.25$ when **e** $\Omega/|J| = 0.0$, **f** $\Omega/|J| = 0.5$, **g** $\Omega/|J| = 1.5$ and (h) $\Omega/|J| = 2.5$. Each curve is associated with one value of the bond dilution concentration p which decreases from 1.0 with the increment of 0.05. Solid lines are the second-order transition lines

of $\Omega/|J|$ (Fig. 3(d)). In Figs. 3(e)-(h), similar trends as those described in Figs. 3(a)-(d) are observed. The main qualitative change is that now, the second-order reentrant behavior appears more pronounced and the magnetic ordering has an expansible tendency. This result may be understood since as t decreases, the proportion of spins influenced by the longitudinal random magnetic field decreases and the ferromagnetic exchange interaction parameter J favors spins to lay in the same direction. The existence of TCP in the model is affected by bond concentration and the strength of the TF. Indeed, for selected values of t, it can be seen from this Fig. 3 that the interval in which TCPs exist, shrinks with increasing $\Omega/|J|$ and disappears when $\Omega/|J|$ is larger than a critical value. According to these figures, one remarks that reentrant phenomena can be only observed for weak values of $\Omega/|J|$.

Fig. 4(a)-(d) shows the reduced critical temperature, $T/|J|$, as a function of the reduced magnetic field $H/|J|$, for $t = 0.5$ and selected values of $\Omega/|J| = 0.0, 0.5, 1.5$ and 2.5. In these figures, the system always undergoes second-order phase transitions, the lines of which depress as H/J increases. Here again, one can also note that reentrant phenomena can be observed for only lower values of the TF. When $\Omega/|J| = 0.0$, (Fig. 4(a)), the phase transition is only of second-order type and $H/|J|$ takes three successive fixed values, 2.0, 4.0 and 6.0 at zero temperature. The second-order reentrant behavior is observed for certain values of the bond concentration p. Indeed, with the decrease in p, the reentrant phenomenon is gradually suppressed until it disappears. It reappears again and is also gradually suppressed till it vanishes again. With nonzero values of $\Omega/|J|$, the phase diagrams exhibit an apparent change with the disappearance of the three successive fixed values of $H/|J|$ at $T/|J| = 0.0$. This is observed in Fig. 4(b) obtained for $\Omega/|J| = 0.5$ where the critical lines show rich variation features with p and reentrant phenomena as observed previously. The corresponding results for $\Omega/|J| = 1.5$ and 2.5 are depicted in Figs. 4(c) and (d), respectively, where the phase diagrams are almost

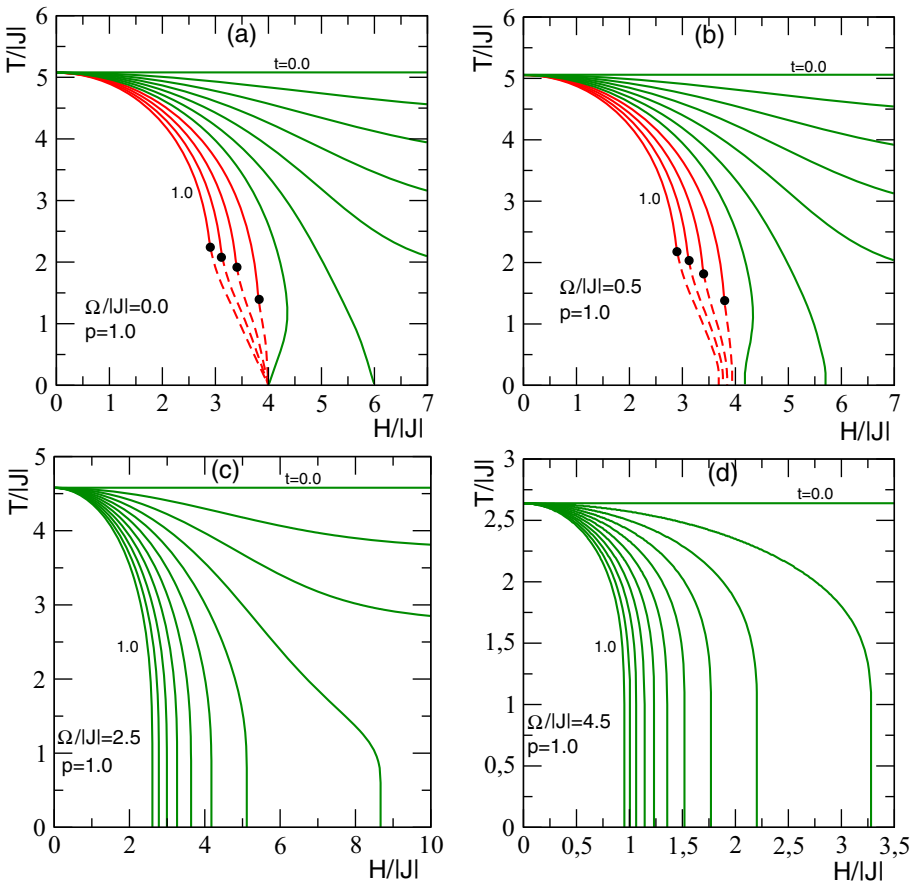

Fig. 5 Phase diagrams of the transverse Ising ferromagnet in a bond diluted and a random longitudinal magnetic field on the ($H/|J|$, $T/|J|$) plane for **a** $\Omega/|J|= 0.0$, **b** $\Omega/|J|= 0.5$, **c** $\Omega/|J|= 2.5$ and **d** $\Omega/|J|= 4.5$. Each curve is associated with one value of the trimodal random concentration t which decreases from 1.0 with the increment of 0.1. Solid (dashed) lines are second- (first) order transition lines. Red ones are associated with phase boundaries with TCPs (circles)

of the same topology. In these phase diagrams, the critical temperatures decrease monotonically as $H/|J|$ increases and the critical lines reach the $H/|J|$ axis at different points for selected values of p. Now, the reentrant behavior is suppressed completely. In Figs. 4(e)-(f), one clearly observes that the magnetic ordering phase region has been magnified at low temperatures with respect to Figs. 4(a)-(d). For $p > p^*$, with p^* a critical value which is $\Omega/|J|$-dependent ($p^* = 0.710$ for $\Omega/|J|= 0.0$), T_c-lines do not reach the $H/|J|$-axis. This implies that the critical temperature is still finite while for $p \leq p^*$, T_c-lines exhibit a monotonic decline and the critical temperatures depress to zero at three fixed points for $\Omega/|J|= 0.0$ and four fixed points for $\Omega/|J|= 0.5$, 1.5 and 2.5. According to Figs. 3 and 4, one deduces that a small value of $\Omega/|J|$ is advantageous for magnetic ordering while a large one favors the disordered phase. A smaller value of t magnifies magnetic ordering phase, while for a larger value of t, the contrary holds.

Fig. 5 illustrates four phase diagrams in the ($H/|J|$, $T/|J|$) plane for $p = 1.0$, varying values of t with selected values of $\Omega/|J|= 0.0$, 0.5, 2.5 and 4.5. It is obvious through these figures that for small values of t, it reduces the phase transition zone of second-order type. The system undergoes for $t = 0.0$ a second-order phase transition whose temperature is not sensitive to the variation of $H/|J|$ as one can expect while it becomes sensitive for $t \neq 0.0$. In Figs. 5(a) and (b), the results show for $t < 0.5$ that the system undergoes only second-order phase transitions and the ground state remains ordered regardless to the field strength $H/|J|$ while for $0.5 \leq t \leq 0.6$, the critical temperature depresses to zero and a reentrant behavior is obtained for appropriate values of t. For $0.6 < t < 1.0$, second-order phase transitions occur and associated temperatures decrease with the increase in $H/|J|$. They change to the first-order phase transitions at TCPs. After that, when $H/|J|$ increases further, the first-order phase transition temperature decreases and vanishes at $H/|J|= 4.0$ (Fig. 5(a)) and also at some other values of $H/|J|$ (Fig. 5(b)) above which only a disordered phase exists. A second-order reentrant behavior is exclusively obtained for $t = 0.6$. It is also important to remark that the critical frontier strongly depends on values of the TF and LF concentration t. By increasing the values of $\Omega/|J|$, the first-order phase transition lines as well as the TCPs disappear (Fig. 5(c)) and the decrease in critical transition temperature is shown. Furthermore, the reentrant behavior does not exist as $\Omega/|J|$ increases to its large values for all selected values of t. It is also easy to understand that the TCP occurs in a certain t range when the reduced field $\Omega/|J|$ has a small value. In Fig. 5(d), one observes that for $t > 0.0$, the critical temperature monotonically decreases with increasing $H/|J|$ and the phase transition lines reach the $T/|J|= 0$-axis at certain values of $H/|J|$, above which disordered phase may exist. It is also important to stress that for sufficiently large values of $\Omega/|J|$, the system does not exhibit first-order phase transitions and TCPs anymore. On the other hand, one only observes that the TF induces a decrease in the transition temperature.

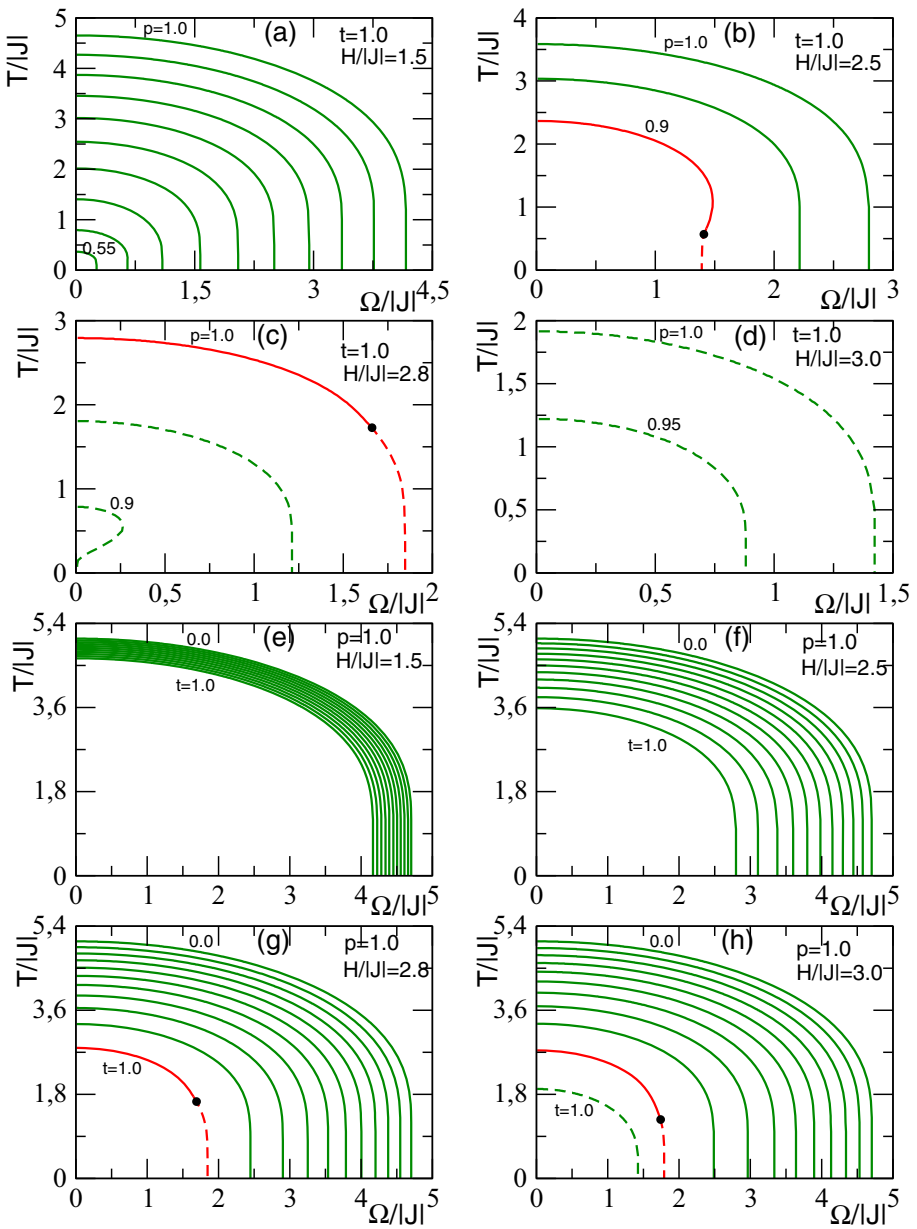

Fig. 6 Phase diagrams of the transverse Ising ferromagnet in a bond diluted and a random longitudinal magnetic field on the $(\Omega/|J|, T/|J|)$ plane for (i) $t = 1.0$ with **a** $H/|J|= 1.5$, **b** $H/|J|= 2.5$, **c** $H/|J|= 2.8$ and **d** $H/|J|= 3.0$. Each curve is associated with one value of the bond dilution concentration p which decreases from 1.0 with the increment of 0.05. (ii) $p = 1.0$ when **e** $H/|J|= 1.5$, **f** $H/|J|= 2.5$, **g** $H/|J|= 2.8$ and **h** $H/|J|= 3.0$. Each curve is associated with one value of the trimodal random concentration t which decreases from 1.0 with the increment of 0.1. Solid (dashed) lines are the second- (first) order transition lines. Red ones are associated with phase boundaries with TCPs (circles)

Fig. 6 illustrates the phase diagrams of the model on the $(\Omega/|J|, T/|J|)$ plane for $t = 1.0$ and selected values of $H/|J|=$ 1.5, 2.5, 2.8 and 3.0 when the values of the bimodal bond dilution concentration p are varied. One can clearly observe that smaller values of $H/|J|$ enlarge the magnetic ordering phase domain (Fig. 6(a)) while larger ones lead to the opposite trend. Indeed, for $H/|J|= 2.5$ and 2.8 corresponding, respectively, to Fig. 6(b) and (c), the ferromagnetic ordering region is shrinking and the system exhibits T_t- and T_c-lines as well as TCPs. The first- and second-order reentrant behaviors are also exhibited. For $H/|J|= 3.0$, only T_t-lines are obtained and the first-order phase transition temperatures depress to zero. When $H/|J|> 3.945$, the system is totally disordered and no phase transition occurs. Fig. 6(e)-(h) expresses the phase diagrams of the model on the $(\Omega/|J|, T/|J|)$ plane for $p = 1.0$ and selected values of $H/|J|= 1.5$, 2.5, 2.8 and 3.0. It emerges that, when the LF takes small values, the phase boundaries are only of the second-order type and the effect of increasing t on transition lines appears to be weak (Fig. 6(e)). For large values of $H/|J|$, the magnetic ordering phase regions shrink with the increase in t and first- and second-order phase transitions as well as TCPs appear for large values of t (Figs. 6(f)-(h)).

5 Conclusion

In this work, we have performed the EFT with correlations calculations to investigate the transverse Ising model with a random bond and a random longitudinal magnetic field. While varying probabilities p and t, related, respectively, to bonds concentration and longitudinal field effect, interesting properties of the model have been discovered. First, the thermal variations of the model order parameters showed rich features. They revealed continuous and discontinuous phase transitions. Second, it has been observed that some ordered phases are embedded in the disordered ones when the temperature increases for appropriate values of other parameters. These observations lead to very rich temperature phase diagrams for the model that we have specified throughout several figures. In the latter, the key features need to be pointed out. Indeed, phase boundaries changed nature at TCPs for appropriate values of model parameters. First- and second-order reentrant phase boundaries have been observed. The rich behavior of the temperature phase diagrams at sufficiently low temperatures brought us to devise the ground state phase one in the $(H/|J|, \Omega/|J|)$ plane for varying t and p to understand the critical behavior of the model in this low-temperature range. Some similarities of these ground state phase diagrams with those illustrated in the $(H/|J|, T/|J|)$ plane have been detected.

Data Availability No Data associated in the manuscript.

References

1. E. Ising, Z. Physik **31**, 253 (1925)
2. L. Bahmad, A. Benyoussef, H. Ez-Zahraouy, J. Magn. Magn. Mater. **238**, 115 (2002)
3. C.T. Bach, N.T. Nguyen, G.H. Bach, J. Magn. Magn. Mater. **483**, 136 (2019)
4. H.-x. Cao, Q. Jiang, C. Xu, Z.-ya Li, Solid State Commun. **103**, 223 (1997)
5. I. Essaoudi, A. Saber, A. Ainane, M. Saber, Phys. Scr. **59**, 168 (1999)
6. T. Kaneyoshi, J. Magn. Magn. Mater. **406**, 83 (2016)
7. T. Kaneyoshi, J. Supercond. Nov. Magn. **30**, 1309 (2017)
8. D.A.. do Nascimento, M.A. Neto, J.R. de Sousa, J.T. Pacobahyba, J. Magn. Magn. Mater. **324**, 2429 (2012)
9. D.A. do Nascimento, J.T. Pacobahybaa, M.A. Neto, O.D.R. Salmon, J.A. Plascak, Physica A **474**, 224 (2017)
10. D.A. do Nascimento, M.A. Neto, J.R. de Sousa, J.T. Pacobahyba, Physica A **392**, 5313 (2013)
11. M.A. Neto, J.R. de Sousa, Physica A **392**, 1 (2013)
12. M. Neto, J.R. de Sousa, Phys. Scr. **87**, 055007 (2013)
13. L. Peliti, M. Saber, Physica A **262**, 505 (1999)
14. J. Geng, G. Wei, J. Magn. Magn. Mater. **321**, 1964 (2009)
15. B. Laaboudi, M. Kerouad, Physica A **250**, 384 (1998)
16. A. Bobák, E. Jurčišinová, M. Jurčišin, M. Žukovič, T. Balcerzak, Physica A **518**, 13 (2019)
17. A. Bobák, E. Jurčišinová, M. Jurčišin, M. Žukovič, Phys. Rev. E **97**, 022124 (2018)
18. E.E. Mir, M. Saber, phys. stat. sol. (b) **183**, 251 (1994)
19. A. Ainane, A. El-Atri, M. Saber, J. Magn. Magn. Mater. **145**, 139 (1995)
20. D.F. de Albuquerque, I.P. Fittipaldi, J.R. de Sousa, Phys. Rev. B **56**, 13650 (1997)
21. V.N. Plechko, Phys. Lett. A **239**, 289 (1998)
22. W. Selke, L.N. Shchur, O.A. Vasilyev, Physica A **259**, 388 (1998)
23. K. Afif, A. Benyoussef, M. Hamedoun, A. Hourmatallah, phys. stat. sol. (a) **171**, 571 (1999)
24. S.M.A. Tabei, M.J.P. Gingras, Y.-J. Kao, P. Stasiak, J.-Y. Fortin, Phys. Rev. Lett. **97**, 237203 (2006)
25. S. Davatolhagh, L. Separdar, M. Barati, Phys. Rev. E **78**, 021138 (2008)
26. A. Dutta, R. Loganayagam, Phys. Rev. B **75**, 052405 (2007)
27. P.E. Theodorakis, N.G. Fytas, Eur. Phys. J. B **81**, 245 (2011)
28. M. Picco, A. Honecker, P. Pujol, Online at stacks.iop.org/JSTAT/2006/P09006
29. N.A. Ridha, M.F. Mustamin, T. Surungan, I.O.P. Conf, Ser. J. Phys. Conf. Ser. **979**, 012086 (2018)
30. Ü. Akinci, J. Magn. Magn. Mater. **343**, 69 (2013)
31. E. Albayrak, Physica A **575**, 126054 (2021)
32. T. Nowotny, H. Patzlaff, U. Behn, Phys. Rev. E **65**, 016127 (2001)
33. A. Rosas, S. Coutinho, Physica A **335**, 115 (2004)
34. D.F. de Albuquerque, I.P. Fittipaldi, J.R. de Sousa, J. Magn. Magn. Mater. **306**, 92 (2006)
35. D.F. de Albuquerque, I.P. Fittipaldi, J.R. de Sousa, N.O. Moreno, Physica B **384**, 230 (2006)
36. K. Bannora, G. Ismail, W. Hassan, Chin. Phys. B (2010) 107501
37. F.F. Doria, R. Erichsen Jr., D. Dominguez, Mario González, S.G. Magalhaes, Physica A **422**, 58 (2015)
38. A. Santos-Filho, D.F. de Albuquerque, J.B. Santos-Filho, T.S.A. Batista, Physica A **461**, 133 (2016)
39. M. Kumar, V. Banerjee, S. Puri, Eur. Phys. J. E **40**, 96 (2017)
40. I.A. Hadjiagapiou, Physica A **390**, 2229 (2011)
41. B. Laaboudi, M. Kerouad, Phys. Scripta **377**, 61 (2000)
42. M. Schechter, Phys. Rev. **77**, 020401(R) (2008)
43. E. Albayrak, J. Phys. Chinese **68**, 100 (2020)
44. E. Albayrak, Mod. Phys. Lett. B **35**, 2150270 (2021)
45. R.A.A. Yessoufou, E. Albayrak, G. Seto, Chin. J. Phys. **77**, 2713 (2022)
46. M. Hasenbusch, F.P. Toldin, A. Pelissetto, E. Vicari, Phys. Rev. E **78**, 011110 (2008)
47. S.-L. Yan, C.-Z. Yang, Solid State Commun. **100**, 851 (1996)
48. R.A.A. Yessoufou, A. Kpadonou, G. Seto, E. Albayrak, Acta Phys. Pol. A **141**, 634 (2022)
49. H.B. Callen, Phys. Lett. **4**, 161 (1963)

50. H. Suzuki, Phys. Lett. **19**, 267 (1965)
51. R. Honmura, T. Kaneyoshi, J. Phys. C: Solid State Phys. **12**, 3979 (1979)
52. T. Kaneyoshi, J.W. Tucker, M. Jascur, Physica A **186**, 495 (1992)
53. F. Zernike, Physica A **7**, 565 (1940)